Journal of Geodynamics 143 (2021) 101810

Contents lists available at ScienceDirect

Journal of Geodynamics

journal homepage: www.elsevier.com/locate/jog

Crustal anisotropy in the southern Aegean from shear wave splitting of local earthquakes

K.I. Konstantinou [a,*], V. Syahra [a], P. Ranjan [a,b]

[a] Dept. of Earth Sciences, National Central University, Jhongli, 320, Taiwan
[b] Taiwan International Graduate Program-Earth System Science (TIGP-ESS), Taipei, Taiwan

ARTICLE INFO

Keywords:
Shear wave splitting
Aegean
Deformation
Crustal anisotropy
Earthquakes, stress

ABSTRACT

In this study, we measured shear wave splitting (fast direction and delay time) from 5193 crustal earthquakes that occurred in the south Aegean that were recorded by 65 stations of the EGELADOS, GEOFON, and MedNet networks between November 2005–January 2007. We utilized the Multiple Filter Automatic splitting Technique (MFAST) that allows quick processing of thousands of events and obtained a total of 3732 high-quality measurements. In general, the majority of fast directions follows a trend of NNE-SSW or NNW-SSE, while the average delay time was found equal to 0.149 s. Analysis of the percentage of anisotropy with hypocentral depth indicates that the interval between 5−20 km exhibits up to 6% of crustal anisotropy with the majority of values being smaller than 4%. Comparison of the observed fast shear wave directions with the maximum horizontal stress (S_{hmax}) shows that stress-induced anisotropy can explain the fast directions along the forearc (Peloponnese, Kythira strait, eastern Crete, Kasos, Karpathos, Rhodes) and SW Turkey. In the Cyclades most fast directions are significantly different from S_{hmax}. Structural anisotropy is dominant in southern Peloponnese, in some parts of Crete and Karpathos. In Cyclades fast directions at several stations agree well with the stretching lineations along the exhumed metamorphic core complex and some major fault zones. A comparison of fast shear wave directions of crustal anisotropy with those of SKS mantle anisotropy shows good agreement in the forearc (Peloponnese, eastern Crete, Karpathos, Rhodes) as well as SW Turkey and suggests that the crust is deforming in the same direction with the mantle flow. This pattern becomes less clear in the Cyclades where stations near the metamorphic core complex exhibit good agreement, while others exhibit large deviations between the two fast directions and point to a possible decoupling of the two lithospheric units.

1. Introduction

The subduction of the African lithosphere beneath the Eurasian plate at a rate of 0.9 cm/yr formed the Hellenic subduction zone along the southern Aegean and is responsible for the observed shallow and intermediate-depth seismicity in this area (Fig. 1) (Papazachos et al., 2000; Reilinger et al., 2010; Floyd et al., 2010; Shaw and Jackson, 2010; England et al., 2016). The strongly curved forearc of the subduction extends along NW-SE direction from Peloponnese, Kythira and Crete changing to NE-SW direction along Karpathos and Rhodes. Crustal seismicity is high along the forearc where occasionally moderate to large events may nucleate, while large thrust earthquakes may occur along the Hellenic, Strabo and Pliny trenches (Shaw et al., 2008; Mouslopoulou et al., 2015; Saltogianni et al., 2020). The Cyclades islands, located to the north of the volcanic arc, essentially represent outcrops of an exhumed metamorphic core complex and are characterized by relatively low levels of crustal seismicity. The southern Aegean upper plate has been subjected to extensional deformation since the Oligocene, as a result of gravitational spreading due to slab rollback (Konstantinou et al., 2016 and references therein). Several studies have tried to investigate the effect of the retreating slab on the long-term deformation of the crust and upper mantle, concluding that both of them have undergone the same direction of flow at least since the Miocene (Brun and Sokoutis, 2010; Endrun et al., 2011; Jolivet et al., 2013).

Seismic anisotropy refers to the phenomenon where shear waves may split into two almost orthogonal polarization phases, one termed as “fast” and the other as “slow” due to their different velocities (Crampin and Chastin, 2003; Crampin and Peacock, 2005). In the upper mantle, rocks may become anisotropic when olivine crystals develop Lattice Preferred Orientation (LPO) during deformation, resulting in the fast

* Corresponding author.
E-mail address: kkonst@cc.ncu.edu.tw (K.I. Konstantinou).

https://doi.org/10.1016/j.jog.2020.101810
Received 7 September 2020; Received in revised form 1 December 2020; Accepted 1 December 2020
Available online 8 December 2020
0264-3707/© 2020 Elsevier Ltd. All rights reserved.

polarization direction aligned with that of maximum shear (Maupin and Park, 2007). Crustal rocks may also display seismic anisotropy either as a result of fluid saturated micro-cracks aligned along the direction of maximum horizontal stress, hereafter referred to as S_{hmax} (Crampin and Peacock, 2008), or due to the preferred orientation of minerals along fault zones, sedimentary layers and metamorphic rocks (Brocher and Christensen, 1990; Boness and Zoback, 2006; Okaya et al., 2018). Subduction zones are attractive targets for studying seismic anisotropy since they exhibit significant long-term deformation over a range of depths, from the upper crust down to the lithospheric upper mantle (e.g., Saiga et al., 2011; Balfour et al., 2012; Huesca-Pérez et al., 2019). Seismic anisotropy can be inferred by applying a variety of methodologies, such as receiver functions or surface waves dispersion, however, the commonest method is the detection of shear wave splitting in recorded waveforms of local/regional and teleseismic earthquakes.

Mantle anisotropy in the southern Aegean has been investigated by a series of studies using teleseismic data recorded by permanent as well as temporary seismic networks (Hatzfeld et al., 2001; Schmid et al., 2004; Paul et al., 2014; Evangelidis et al., 2011, 2017). On the contrary, crustal anisotropy has received much less attention with only few studies reporting shear wave splitting measurements around the Corinth rift (Giannopoulos et al., 2015; Kaviris et al., 2017), the Marathon area near Athens (Kaviris et al., 2018) and the Santorini caldera (Konstantinou et al., 2013; Kaviris et al., 2015). Although spatially limited, the results of these studies indicate that crustal anisotropy is caused by a combination of the present-day stress field, structural features, and in volcanic areas by the presence of transient deformation sources. In this work, we utilize high-quality waveform data recorded in the southern Aegean by a dense temporary network in order to obtain shear wave splitting parameters (fast direction, delay time) from local earthquakes and investigate the causes of crustal anisotropy. First, we give a brief description of the seismic network and of the procedure that was followed for the detection of events as well as the calculation of absolute earthquake locations. The methodology for estimating shear wave splitting parameters is then outlined along with the criteria for selecting the best quality measurements. The spatial distribution of the splitting parameters is subsequently correlated with the present-day stress field and structural features of the southern Aegean in an effort to decipher the influence of these factors on crustal anisotropy. Finally, we discuss the relationship between crustal and SKS mantle anisotropy as a means of investigating the coherence of lithospheric vertical deformation in the southern Aegean.

2. Data and earthquake locations

EGELADOS (Exploring the GEodynamics of subducting Lithosphere using an Amphibian Deployment Of Seismographs) was a temporary seismic network consisting of both land and ocean bottom seismographs which operated from October 2005 until March 2007 (Friederich and Meier, 2008). The network consisted of 56 land-based stations and covered the entire southern Aegean from Peloponnese in the west to southwestern Turkey in the east, as well as many of the smaller islands in the Cyclades (Fig. 2). The majority of these stations were equipped with broadband sensors such as Güralp 60 s and STS-2 seismometers, while only seven stations were equipped with short-period 1 Hz Mark sensors. Data recorded during the same period by 8 permanent broadband stations of the GEOFON seismic network and one station of the MedNet network were also incorporated in the EGELADOS dataset. Inclusion of data from the ocean bottom seismographs that were deployed south of Crete was not possible as they all stopped working shortly after deployment.

For the purposes of this study we considered data from November 2005 until January 2007 which covers the period when all aforementioned stations were fully operational. Initially, automatic event

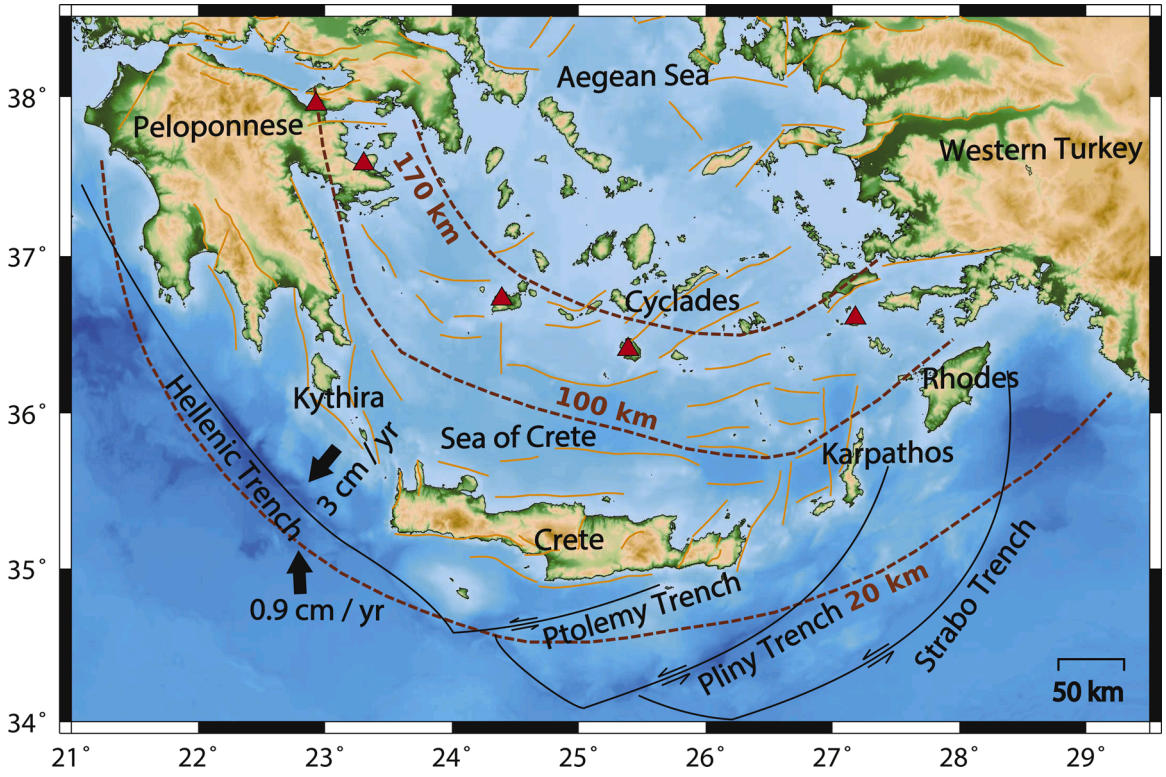

Fig. 1. Simplified tectonic map of the south Aegean. The black arrows and values near each arrow represent the direction and velocity of plate motion relative to Eurasia (McClusky et al., 2000). The orange lines represent the active faults that have been extracted from the Greek Database of Seismogenic Sources (GreDaSS) (Caputo and Pavlides, 2013). The red triangles represent active volcanoes. The brown dashed lines indicate the isodepth curves of the Wadati-Benioff zone (Papazachos et al., 2000). (For interpretation of the references to colour in this figure legend, the reader is referred to the web version of this article.)

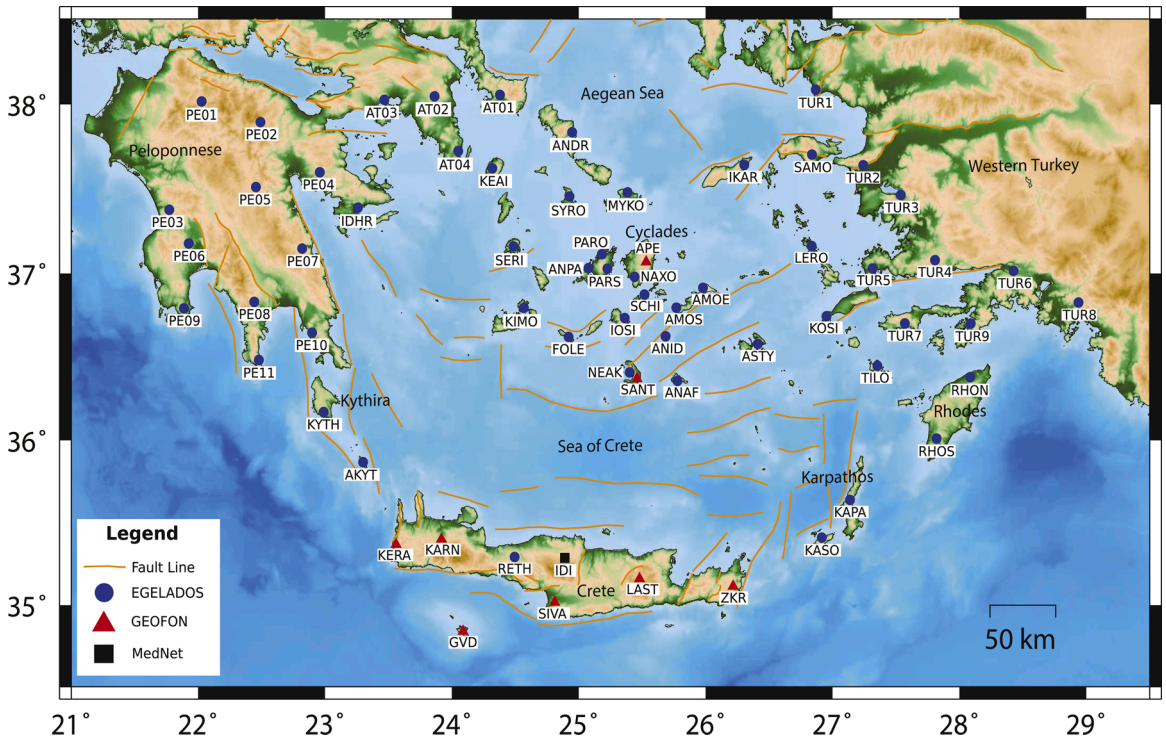

Fig. 2. Map of station distribution of EGELADOS temporary seismic network along with the additional stations of GEOFON and MedNet networks.

detection and picking of P phases was performed, followed by manual checking of the automatic picks and the careful manual picking of S phases. A total of 6316 earthquakes were detected and picked in this way, representing both shallow and intermediate-depth seismicity. We calculated the absolute locations of all events by utilizing the NonLinLoc package (Lomax et al., 2009) which implements a nonlinear probabilistic algorithm along with the Oct-Tree searching method (Lomax and Curtis, 2001). NonLinLoc can be used with any velocity model (1D or 3D) and provides comprehensive uncertainty and resolution information represented by the posterior density function. The minimum 1D velocity model of Brüstle (2012), derived from the inversion of EGELADOS travel time data, was utilized in order to calculate theoretical travel times (Table 1). The average horizontal and vertical uncertainty of these locations were found to be 4.1 km (±4.1 km) and 4.6 km (±3.3 km), while the average root mean square (rms) residual was 0.28 s (±0.12 s). Histograms describing the distribution of these uncertainties and rms residuals can be found in Fig. S1 of the Supplementary material. The thickness of the crust in our study area varies from about 24 km–33 km (Sodoudi et al., 2006), therefore from the initial 6316 earthquakes we selected 5193 events with hypocentral depths of less than 30 km for further analysis.

Table 1
Minimum 1D velocity model utilized in this study (from Brüstle, 2012).

Depth (km)	Vp (km/s)	Vs (km/s)
0	5.74	3.08
5	5.89	3.38
10	5.89	3.45
15	5.91	3.45
20	6.23	3.77
25	6.26	3.93
30	7.53	4.10
35	7.55	4.10
40	7.86	4.56
50	7.92	4.59
70	8.13	4.68
100	8.42	4.91
150	8.43	4.91
200	8.43	4.91

3. Shear wave splitting measurements

The waveforms of the selected earthquakes were further processed with the Multiple Filter Automatic Splitting Technique (MFAST) package (Savage et al., 2010). MFAST has the advantage of allowing the quick processing of thousands of events and uses the algorithm of Silver and Chan (1991) for calculating the splitting parameters (i.e. fast direction ϕ and delay time δt). The problem of the dependence of such measurements on the filter used and the chosen time window is circumvented in MFAST by the use of cluster analysis (Teanby and Kendall, 2004), where the most stable result is obtained by finding the optimal filter and measurement window. This task is accomplished by measuring splitting parameters over multiple time windows and by using a set of predefined filters for the purpose of finding the frequency band with the largest signal-to-noise ratio (SNR). The cluster of measurements with the smallest variance is chosen as the best cluster and the measurement that is designated as "final" is the one that exhibits the smallest error in splitting parameters within this cluster.

In this study, we chose a set of 14 bandpass filters with lowest corner frequencies between 0.1−1 Hz and highest ones from 5 to 10 Hz (Table S1 in Supplementary material) that have been shown to be suitable for analyzing local/regional waveforms in previous crustal anisotropy studies (Audoine, 2002; Hu et al., 2020). The SNR of the filtered data was calculated using the same 3 s window length for both noise and signal. The noise window precedes the S arrival time and includes an offset in order to take into account any uncertainty in the S phase pick. The length of each measurement window was calculated based on the dominant frequency (f_d) of the signal. The minimum window length was chosen to be one period long ($\sim 1/f_d$), while the maximum value for the window length was 2.5 times the minimum window length. If the S phase recorded at any station had an incidence angle greater than 35°, then it was not selected for analysis in order to avoid distortions generated by S-P conversions at the surface. MFAST automatically assigns a quality label to each final measurement that may

range from A to D, signifying best and worst qualities respectively. Assignment of the first two qualities (A and B) is made based on whether the measurement is within a cluster of quality Acl and Bcl as well as the values of SNR and the 95 % confidence interval of the ϕ measurement ($\delta\phi$). Quality A conforms to the criteria of SNR > 4 and $\delta\phi < 10^{\circ}$, while quality B corresponds to SNR > 3 and $\delta\phi < 25^{\circ}$; an example of a quality A measurement can be seen in Fig. 3.

After the processing of all available data, MFAST yielded a total of 7962 splitting measurements of which we selected 3732 quality A and B measurements for further analysis. Fig. 4 shows the distribution of the crustal earthquakes whose waveforms were used for splitting measurements, along with the stations that are colored based on the total

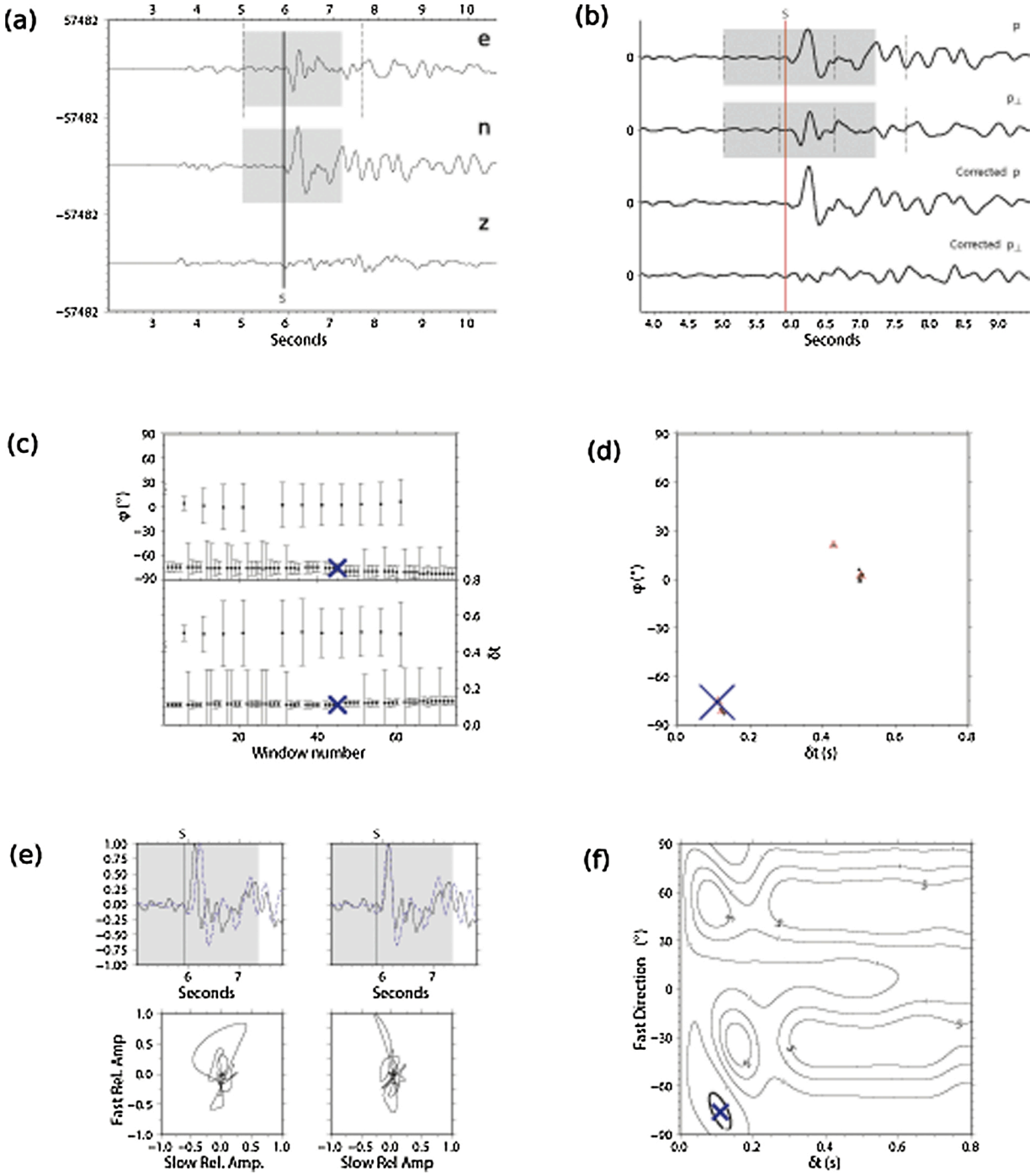

Fig. 3. An example of quality A measurement of an event recorded 7 January 2006 (16:06 UTC) at station TUR4. Red lines mark the S-phase pick and grey boxes in panels (a), (b) and (e) show the time window used for measurement. Black dashed lines are the minimum start and maximum end times for windows used in the processing (panels a and b). (a) waveforms bandpass filtered between 0.1–1 Hz, (b) rotated components before and after correction for anisotropy, (c) fast direction and delay time determined for each measurement window as a function of window number; blue crosses indicate optimal values of ϕ and δt, (d) cluster measurements with the blue large cross being the chosen cluster, (e) waveform and particle motion uncorrected (left) and corrected (right) for anisotropy according to the final chosen window, (f) contours of the smallest eigenvalue of the covariance matrix for the final chosen measurement; the blue large cross in this measurement marks the best splitting parameter (in this case $\phi = 76^{\circ}$, $\delta t = 0.11$ s). (For interpretation of the references to colour in this figure legend, the reader is referred to the web version of this article.)

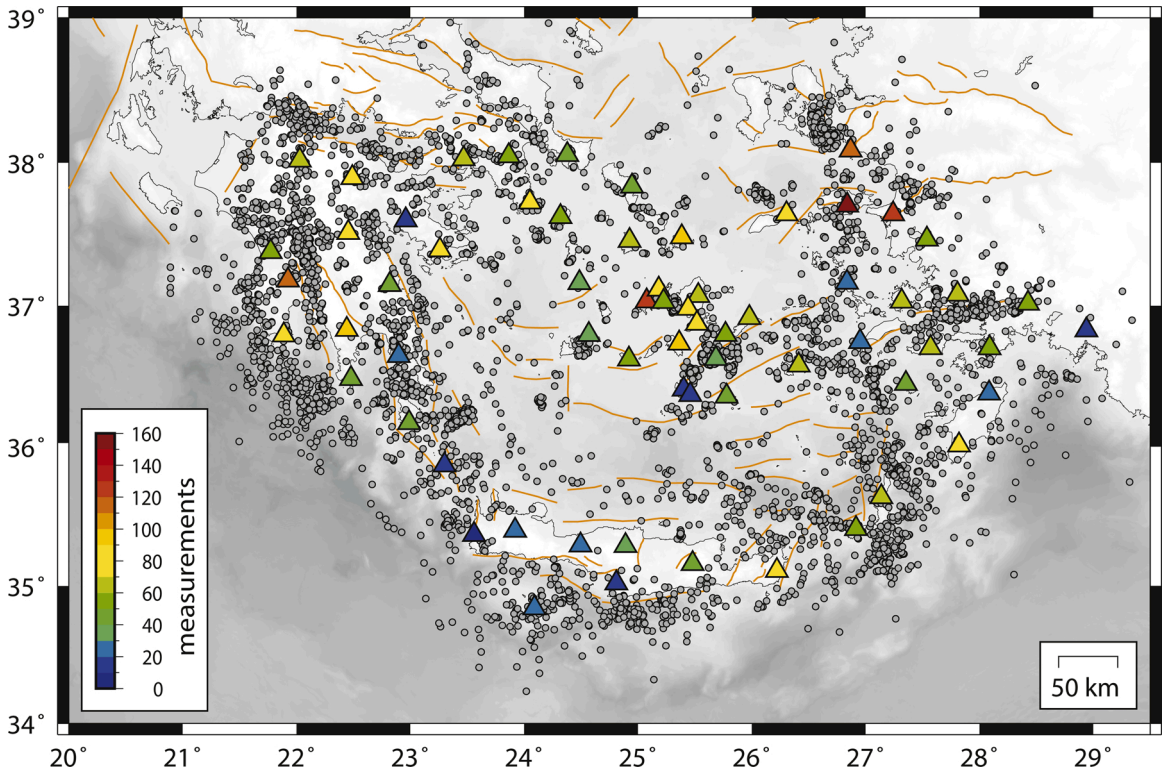

Fig. 4. Map showing the total number of shear wave splitting measurements per station. The grey circles represent the NonLinLoc locations of the events that were used for measuring splitting parameters. Other symbols are the same as in Fig. 1.

number of observations each one yielded. As it can be seen the majority of the stations are associated with a large number of splitting measurements in the range of 30–100, while five of them produced more than 120 measurements and about ten stations, located mostly in SE Peloponnese/western Crete, produced 10–30 measurements. The next step was the statistical analysis of both the fast axis orientation ϕ and the delay time δt at each station. We first calculated the mean resultant length R (Mardia and Jupp, 2000) as a means of investigating the variance of the fast directions in each station. R takes values from 0 to 1 with the former value indicating large scatter and the latter value representing data clustered around a dominant direction. The smallest R value can be found at station TUR8 (~0.44) and the largest one (~0.84) at station KERA, while all stations except from TUR8 and NEAK exhibited R values higher than 0.5 indicating small variance in ϕ. We also formally tested the significance of ϕ variations at each station using the Rayleigh test (Trauth, 2010) that utilizes the null hypothesis that the sample of ϕ measurements is drawn from a population of orientations uniformly distributed around a circle (i.e. there is no preferred direction). The test produces a p-value that is compared to the significance level in order to decide whether or not to reject the null hypothesis. The obtained p-value at each station was found to be much smaller than 0.05 (95 % confidence level) leading to the rejection of the null hypothesis and indicating that the data at each station show a preferred direction. The mean direction at each station can then be calculated as

$$\phi_{mean} = \operatorname{atan}\left(\frac{\sum_{i=1}^{N} \omega_i \sin\phi_i}{\sum_{i=1}^{N} \omega_i \cos\phi_i}\right)\frac{180}{\pi} \quad (1)$$

where ϕ_i represents the i-th fast direction value at that particular station, N is the number of observations, and the individual weights ω_i can be calculated using the following expression

$$\omega_i = \frac{1/\sigma_{\phi_i}^2}{\sum_{i=1}^{N} 1/\sigma_{\phi_i}^2} \quad (2)$$

where σ_{ϕ}^2 represents the uncertainty of the i-th individual fast direction. We calculated mean fast directions at each station by utilizing both Eqs. (1) and (2). On the other hand, mean delay times were found to vary from a minimum of 0.08 s (station IOSI) to a maximum of 0.19 s (stations KAPA, KERA, TUR2). Table S2 in the Supplementary material contains all the information related to the 3732 high-quality measurements, while Table S3 summarizes the results for R values, the Rayleigh test and the mean ϕ direction/delay time per station using Eqs. (1) and (2).

Another aspect of shear wave splitting is "null" measurements, a term that refers to the situation when either there is no anisotropy in the plane of the S phase particle motion, or the initial polarization of the shear wave is parallel to the fast or slow direction (Silver and Chan, 1991; Wüstefeld and Bokelmann, 2007). MFAST considers a measurement to be null when the resulting delay time is equal to zero and the absolute difference between ϕ and the initial polarization of the shear wave is either $\geq 70^\circ$ or $\leq 20^\circ$. In this study, we identified in total 1942 null results at 65 stations that are provided in Table S4 of the Supplementary material that accompanies this work. Null measurements can be used to check the validity of the mean fast directions calculated previously. The mean fast direction can be considered robust if the null measurements are either aligned parallel to it and/or they are aligned in a perpendicular direction. Fig. S2 in the electronic supplement shows rose diagrams where the null measurements have been plotted at each station along with the mean fast direction. As it can be seen, for the majority of the stations the null measurements are almost parallel and/or perpendicular to the mean fast direction.

In order to visualize the spatial variation of the measured fast directions, we plotted rose diagrams for each station on the map, also highlighting the calculated mean fast direction (Fig. 5). In northern Peloponnese we observe that some fast directions are trending approximately NNE-SSW/NE-SW (PE01, PE03, PE05, PE07), whereas in the south the orientation changes to NNW-SSE/NW-SE (PE09, PE08, PE11). Stations in Crete exhibit a more complex pattern, with fast directions in four stations (KERA, RETH, LAST, SIVA) trending NNW-SSE/NW-SE,

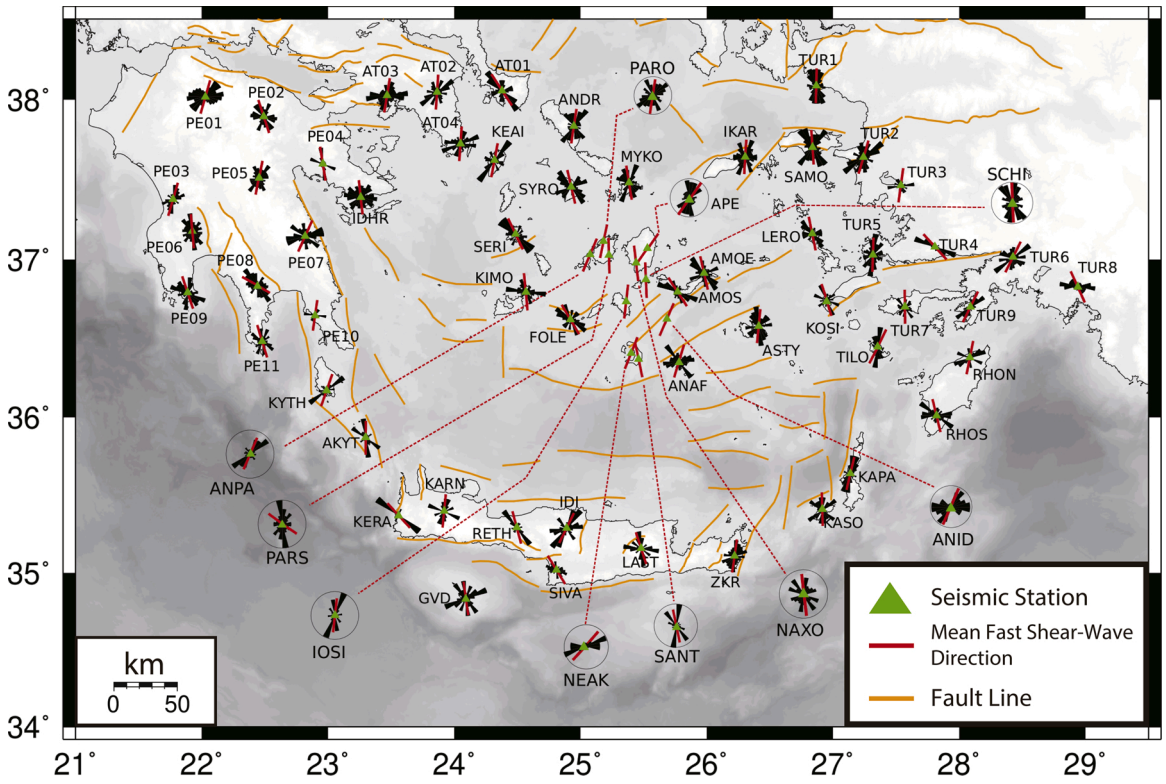

Fig. 5. Map of fast shear wave directions in the south Aegean determined by using MFAST. Black rose diagrams are plotted on each station and scaled according to the number of measurements. The red solid bars inside the rose diagrams are the calculated mean fast directions (see text for more details). (For interpretation of the references to colour in this figure legend, the reader is referred to the web version of this article.)

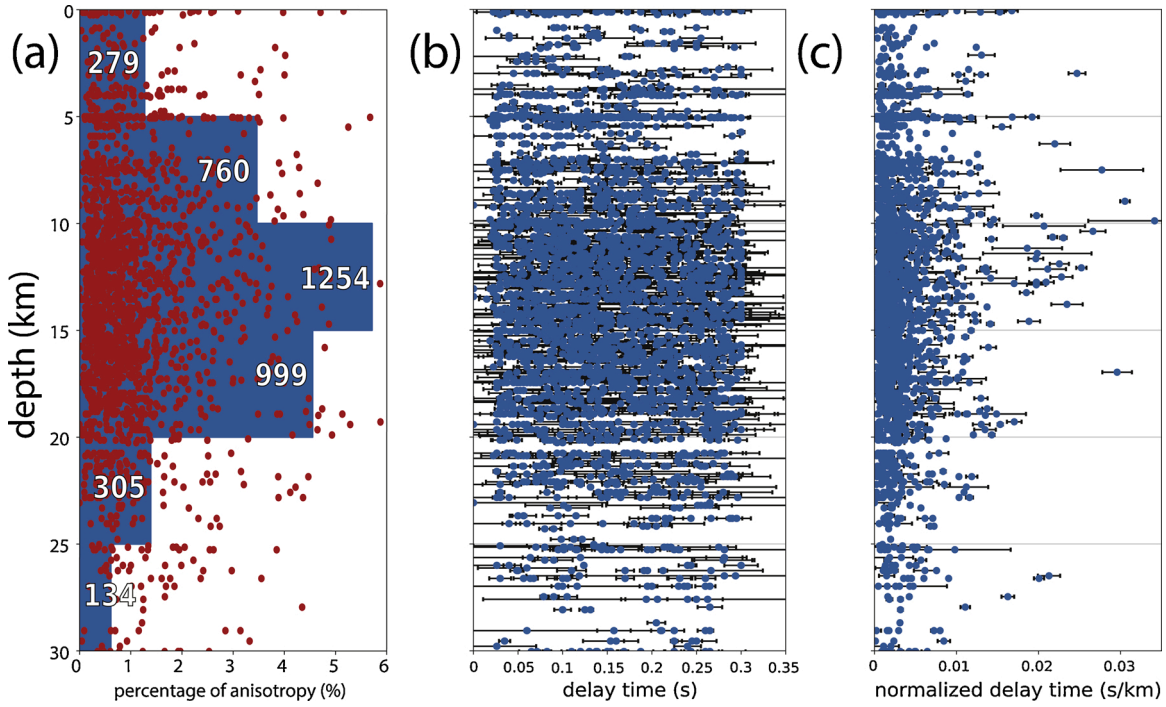

Fig. 6. Summary of the variation of shear wave anisotropy with depth in the southern Aegean. (a) histogram that shows the distribution of hypocentral depth with superimposed the percentage of anisotropy of each measurement as red dots; the numbers in white fonts represent the total number of measurements in each bin, (b) & (c) panels show the variation of delay time and normalized delay time versus hypocentral depth for all high-quality measurements. (For interpretation of the references to colour in this figure legend, the reader is referred to the web version of this article.)

whereas at another four (GVD, KARN, ZKR, IDI) fast directions are trending NNE-SSW. Further to the east, at stations in the islands of Karpathos and Kasos the fast directions are trending NNE-SSW/NE-SW, while in Rhodes and along the Turkish coast stations exhibit a N-S trend occasionally perturbed towards NE or NW. In the Cyclades the fast directions can be grouped in two orientations, namely NNE-SSW (typical examples are APE, IOSI, ASTY, PARO) and NNW-SSE or NW-SE as in the case of stations such as SERI, KIMO, FOLE and AMOS. In the next sections we will attempt to investigate the causes of crustal anisotropy in the southern Aegean by considering the relationship of our results with the regional stress field and the tectonic characteristics of the area.

4. Discussion

4.1. Depth distribution of anisotropy

As mentioned earlier, the selected earthquakes used for measuring shear wave splitting had hypocentral depths of less than 30 km. In order to investigate the relationship between depth and anisotropy, we first constructed a histogram of depth distribution for the high-quality measurements using a bin size of 5 km which is proportional to the average vertical uncertainty (Fig. 6a). The majority of the measurements (~80 %) are clustered in the depth range of 5–20 km which extends from the brittle seismogenic upper crust to the progressively ductile lower crust. The amount of seismic anisotropy is then quantified by calculating the percentage of anisotropy ξ for each measurement (Savage, 1999).

$$\xi = [(\delta t \times Vs)/d] \times 100\ \% \quad (3)$$

δt is the measured delay time, d is ray path length and Vs is the average shear wave velocity at the hypocentral depth estimated at 5 km intervals from the velocity model of Brüstle (2012) (cf. Table 1). These anisotropy percentages are also plotted in Fig. 6a where it can be seen that the maximum value of ξ does not exceed 6%. We observe that the majority of the measurements exhibit anisotropy percentages of less than 4% without displaying any significant variation with depth. On the other hand, a plot of the delay time versus depth exhibits large scatter (Fig. 6b), which is a recurrent observation in crustal anisotropy studies (Crampin et al., 2004; Peng and Ben-Zion, 2004; Cochran et al., 2006). The normalization of the delay time by dividing it with the ray path length decreases the scatter significantly and confirms the results we obtained for the anisotropy percentage (Fig. 6c). The average normalized delay time is found equal to 0.0035 s/km with the majority of measurements being smaller than 0.01 s/km. The results presented here are in general agreement with those published previously by Endrun et al. (2011) and Cossette et al. (2016) for the area of the Cyclades. The former study utilized 12–18 s period surface waves and observed a percentage of anisotropy of up to 3.5 %, while the latter one used receiver functions and found a percentage of up to 5%. These anisotropy percentages are below the limit of 5.5 % that marks the boundary between intact and heavily fractured rock (Crampin and Peacock, 2008). Considering that for the majority of our measurements anisotropy is below 3%, we can conclude that the upper and lower crust in the southern Aegean consist of rocks that are not heavily fractured. This conclusion also agrees with the observation that most large earthquakes in this area nucleate at 10–15 km depth, suggesting that rock integrity is high enough to allow the rupture to develop and propagate.

4.2. Possible causes of crustal anisotropy

One possible cause of crustal anisotropy is the influence of the regional stress field which promotes the alignment of microcracks and/or pores along a particular direction, a phenomenon that is often referred to as stress-induced anisotropy (Johnson et al., 2011). In order to investigate to what extent crustal anisotropy in the southern Aegean is stress-induced, we utilized the regional stress field model of Konstantinou et al. (2016) that is derived from the inversion of a large number of earthquake focal mechanisms. We determined the direction of S_{hmax} using the method of Zoback (1992), which classifies the stress field into five regimes by using the plunges of the σ_1, σ_2 and σ_3 axes. Our S_{hmax} directions are in agreement with those published recently by Kapetanidis and Kassaras (2019) for the southern Aegean (see Fig. S3 in the electronic supplement). Fig. 7 shows a map where the deviation of the mean fast direction from the direction of S_{hmax} is represented in each station by a rotational wedge. The wedges can be grouped into four classes based on the amount of the deviation they exhibit, ranging from less than 20° to more than 60°. As it can be seen the majority of the stations in Peloponnese agree well with the direction of S_{hmax} (within ~11° to 26°) with only one station exhibiting a larger angular difference (~56°). A similar agreement can be observed along the Kythira straight, Karpathos, Kasos and Rhodes. Most stations along the Turkish coast also exhibit small angular differences below 30° with the exception of two stations where the disagreement is in the order of more than 60°. Stations on the island of Crete show larger angular differences (>60°) especially in the western part and in Gavdos island. At this point it should be noted that the stress field model of Konstantinou et al. (2016) does not include the Cyclades, since there were too few focal mechanisms available in that area for performing stress inversion. However, an extrapolation of S_{hmax} directions in the Cyclades shows an almost E-W orientation (cf. Fig. S3) which would produce deviations >60° for most of the stations there, signifying that stress-induced anisotropy cannot explain the mean fast directions.

Crustal anisotropy may also be induced by the shear rock fabric of fault zones or by the foliation of metamorphic rocks, a phenomenon that is referred to as structural anisotropy (e.g., Okaya et al., 2018). In this sense, if a station is located close to a fault, then the observed anisotropy is expected to be influenced by this structure. In order to investigate this further, we utilized the faults contained in the Greek Database of Seismogenic Sources (GreDaSS) (Caputo and Pavlides, 2013). As previously, Fig. 8 shows a map of rotational wedges describing the angular deviation between the mean fast direction of anisotropy and the strike of the fault that is closest to the station (i.e. within a range of few km). We can observe good agreement at stations in eastern/southern Peloponnese, Crete, Kasos and Karpathos islands with angular deviations in the order of <30°. A comparison between Figs. 7 and 8 reveals that the stations located in the forearc exhibit crustal anisotropy that is influenced by both the present-day stress field and structural features, with the latter being more dominant in Peloponnese. Most of the stations in the Cyclades have large angular deviations (~78°) indicating that fault zones contribute very little to the observed anisotropy. Exceptions to this trend are stations FOLE, IOSI and ANID that exhibit angular deviations of ~27° where fast directions appear to be influenced by the NE-SW faults of the Santorini-Amorgos zone. Several stations (KEAI, ANDR, MYKO, NAXO, APE, PARS) are located on the exhumed metamorphic core complex of the Cyclades, whose exhumation took place during the Miocene (Jolivet et al., 2009). For these stations, we compared the mean fast directions with the stretching vectors (uncorrected for paleomagnetic rotations) of the metamorphic core complex. It can be seen that there is a very good agreement between the two directions, producing angular deviations in the order of less than 30° with the exception of station NAXO where the deviation exceeds 40° (cf. Fig. 8). This indicates that old ("frozen") structure is influential on crustal anisotropy observed in stations at/near the metamorphic core complex.

4.3. Comparison with SKS mantle anisotropy

One advantage of using the EGELADOS data for measuring crustal anisotropy is that mantle anisotropy has been also measured at the same set of stations. More specifically, Evangelidis et al. (2011) utilized waveforms of teleseismic events in order to measure SKS splitting

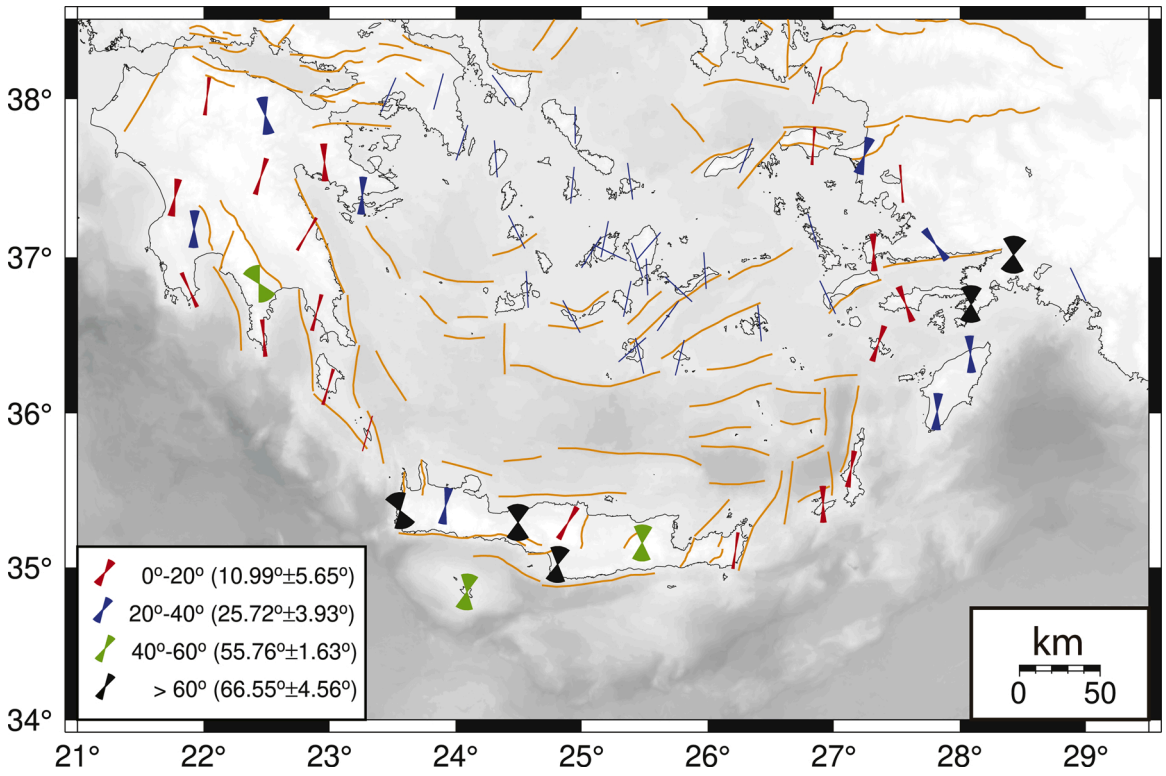

Fig. 7. Comparison of shear wave splitting results with the regional stress field derived by Konstantinou et al. (2016). Rotational wedges show the angular difference between the mean fast direction and maximum horizontal stress at stations where both measurements are available. The angular difference follows the color scheme shown at the lower left hand corner of the map. The average angular difference and its standard deviation are also shown in brackets. In the Cyclades there are no estimates of maximum horizontal stress (see text for details).

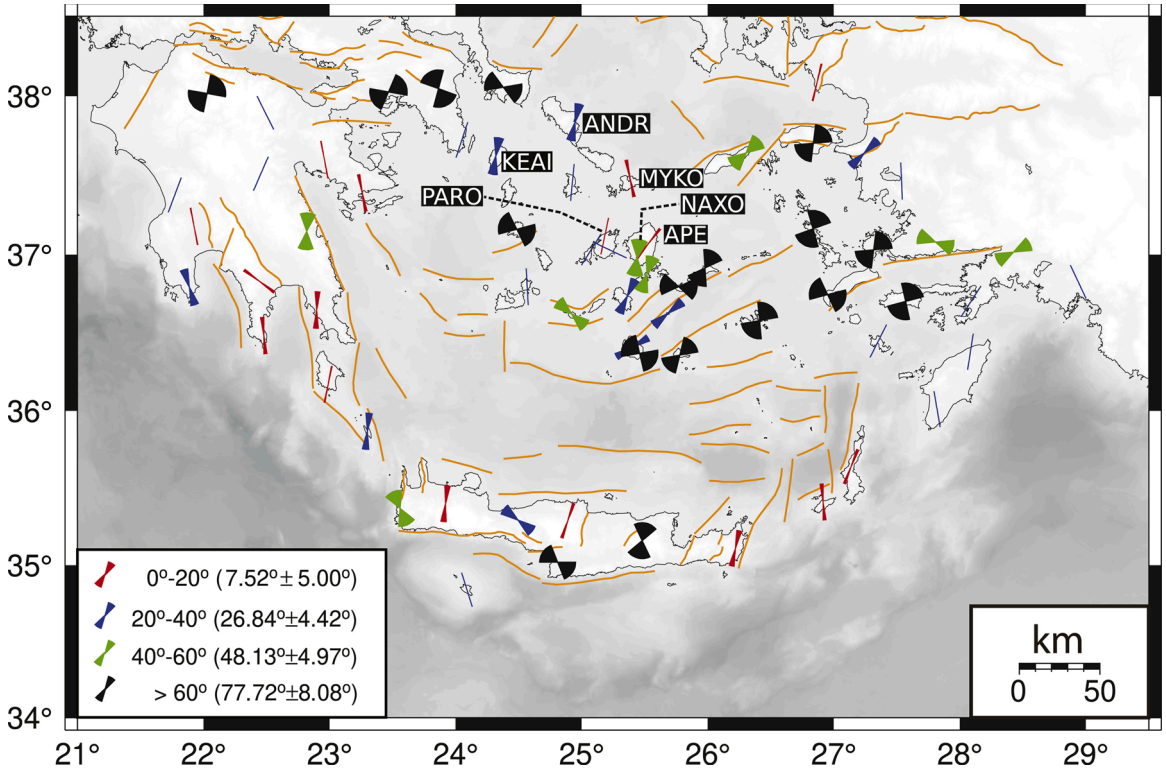

Fig. 8. Comparison of shear wave splitting results with structural features in the south Aegean. Rotational wedges show the angular difference between the mean fast direction and the strike of active faults from the GreDaSS database. At stations that are highlighted by their station code the rotational wedge represents the angular difference between the mean fast direction and the stretching lineations of the metamorphic core complex (Jolivet et al., 2009). All other symbols are the same as in Fig. 7.

parameters in the broader Aegean area and to infer the sources of mantle anisotropy. This allows us to compare our results with those obtained for the anisotropy in the mantle and assess the coherency of the vertical deformation in the lithosphere of the southern Aegean. For this comparison we again make use of rotational wedges that indicate the angular difference between the average fast direction of anisotropy in the crust and the average fast direction of anisotropy in the mantle provided by Evangelidis et al. (2011). Fig. 9 shows a map of these rotational wedges for a total of 39 stations where both kinds of measurements are available.

In previous studies along subduction zones it was found that fast SKS directions generally tend to orientate parallel to the trench, while in the backarc the orientation becomes perpendicular to the trench (Long, 2013). The volcanic arc then serves as a transitional zone between the two, where fast SKS directions form oblique angles with the strike of the trench. As outlined by Evangelidis et al. (2011), this simple pattern of mantle anisotropy cannot fully describe the SKS observations in the southern Aegean owing to the curved geometry of the subduction zone and the strong lateral variations in velocity structure. A number of stations (N = 17) in Peloponnese, the Cyclades, Karpathos, Rhodes and SW Turkey exhibit angular differences between crustal and mantle anisotropy of 30° or less. There is good agreement (10°–30°) between the two fast directions for most of the stations that lie in the forearc and SW Turkey, with some exceptions (KARN, RETH, GVD, RHOS, TUR4, TUR3) where the angular deviation is between 47°–72°. The situation in the Cyclades is more complicated, with some stations exhibiting small (≤30°) angular difference (PARO, ANPA, APE, IOSI, AMOE, SYRO) while at all other stations the disagreement between the two fast directions is significant (≥40°). The former group of stations coincides with part of the exhumed metamorphic core complex and at some of these stations fast directions of crustal anisotropy also agree with the stretching vectors as discussed in the previous section (cf. Fig. 8).

We can conclude therefore that in the forearc area there is enough evidence to support coupling between the mantle flow and the crustal deformation. This conclusion does not seem to hold for western Crete where angular deviations are larger, probably due to the fact that western Crete has likely entered a continental collision stage and its crust exhibits significant structural inhomogeneity (Ranjan et al., 2019). This may also be the reason for the SKS fast directions being almost perpendicular to the trench rather than parallel, in contrast to what can be seen in Kasos, Karpathos and Rhodes (cf. Fig. 9). Endrun et al. (2011) suggested that the observed anisotropy in the Cyclades indicates fossil fabric in the lower crust that was attained during lithospheric extension in the Miocene which was not overprinted owing to the very small present-day strain rates there. Such a suggestion implies coupling between the crust and the lithospheric mantle, which can be seen in some stations exhibiting small angular deviations. However, most of the stations in Cyclades do not follow this trend, which may indicate either decoupling of the two units, or that crustal anisotropy is influenced by post-Miocene tectonic structure in the upper crust.

5. Conclusions

We studied crustal anisotropy in the southern Aegean using a dataset of 5193 local earthquakes that were recorded by 65 EGELADOS/GEOFON/MedNet seismic stations during November 2005 – January 2007. By utilizing the well-known MFAST automatic shear wave splitting methodology we were able to extract a total of 3732 splitting parameters. The results presented in this work are novel for the southern Aegean not only on account of their quantity, but also their quality which is evaluated through well-defined criteria, hence our results are fully reproducible. The main conclusions of this study can be summarized as follows:

1 Variation of the percentage of anisotropy with hypocentral depth indicates that the depth interval between 5−20 km exhibits up to 6 %

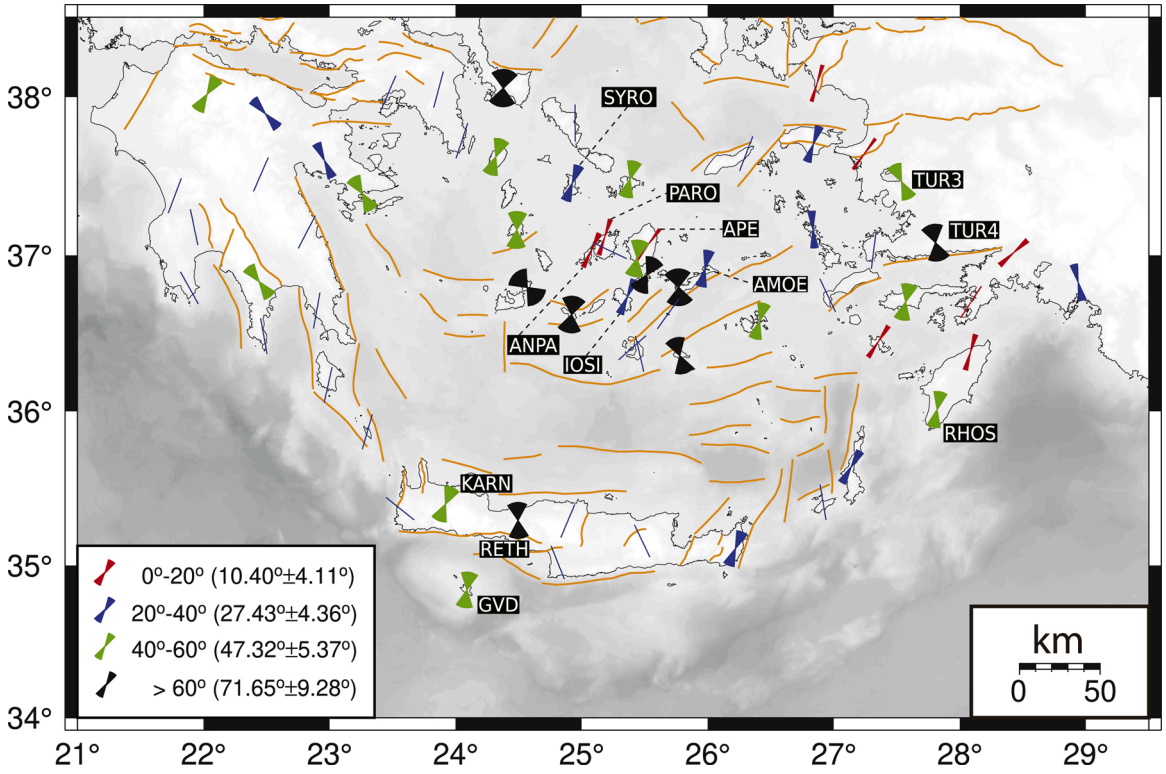

Fig. 9. Comparison between crustal and SKS mantle anisotropy in the south Aegean. Rotational wedges indicate the angular difference between the mean fast direction of crustal anisotropy determined in this study and the mean fast direction of SKS mantle anisotropy (Evangelidis et al., 2011). Station codes mentioned in the text are also highlighted on the map. All other symbols are the same as in Fig. 7.

of crustal anisotropy. The average value of the delay time is equal to 0.149 s while the average normalized delay time is 0.0035 s/km. The low values of anisotropy percentage (<4 %) in most measurements indicate that the upper and lower crust in the south Aegean consists of rocks that are not heavily fractured and maintain a high degree of integrity allowing large ruptures to propagate through them.

2 Comparison of the observed fast shear wave directions with the maximum horizontal stress (S_{hmax}) derived from the model of Konstantinou et al. (2016) shows that stress-induced anisotropy can explain the fast directions along the the forearc (Peloponnese, Kythira strait, eastern Crete, Karpathos, Rhodes) and SW Turkey. In the Cyclades the majority of fast directions are significantly different from S_{hmax}.

3 Structural anisotropy, induced by rock fabric along fault zones near stations, can explain the origin of crustal anisotropy in southern Peloponnese, as well as in some parts of Crete and Karpathos. In the Cyclades the fast directions at several stations agree well with the stretching lineations along the exhumed metamorphic core complex and some major fault zones such as Santorini-Amorgos, hence anisotropy there can be considered also of structural origin.

4 A comparison of fast shear wave directions of crustal anisotropy with those of SKS mantle anisotropy for the same set of stations shows good agreement in the forearc (Peloponnese, eastern Crete, Karpathos, Rhodes) as well as SW Turkey and suggests that the crust is deforming in the same direction as the mantle flow. This conclusion becomes less clear in the Cyclades where stations near the metamorphic core complex exhibit good agreement, while others exhibit large deviations between the two fast directions and point to a possible decoupling of the two lithopsheric units.

Author contribution

K. I. Konstantinou conceived the project, supervised the analysis and wrote the manuscript. V. Syahra and P. Ranjan collected the data and performed the necessary calculations. All authors read the manuscript and contributed in the interpretation of the results.

Declaration of Competing Interest

The authors report no declarations of interest.

Acknowledgments

The first author would like to thank the Ministry of Science and Technology of Taiwan (MOST) for the financial support of this study. Vanisa Syahra held a scholarship from the School of Earth Sciences while studying for a graduate degree at National Central University. The waveforms recorded by EGELADOS can be downloaded from GFZ, Postdam, European Integrated Data Archive (EIDA) website (http://eida.gfz-postdam.de/webdc3) with the network code Z3. We would like to thank the Editor-in-Chief Irina Artemieva for handling our manuscript and two anonymous reviewers for their constructive comments.

Appendix A. Supplementary data

Supplementary material related to this article can be found, in the online version, at doi:https://doi.org/10.1016/j.jog.2020.101810.

References

Audoine, E., 2002. Upper Mantle and Crustal Seismic Anisotropy Across the Pacific-Australian Plate Boundary, New Zealand. PhD thesis. Victoria University, Wellington.

Balfour, N.J., Cassidy, J.F., Dosso, S.E., 2012. Crustal anisotropy in the forearc of the northern Cascadia subduction zone, British Columbia. Geophys. J. Int. 188, 165–176. https://doi.org/10.1111/j.1365-246X.2011.05231.x.

Boness, N.L., Zoback, M.D., 2006. Mapping stress and structurally controlled crustal shear velocity anisotropy in California. Geology 34, 825–828. https://doi.org/10.1130/G22309.1.

Brocher, T.M., Christensen, N.I., 1990. Seismic anisotropy due to preferred mineral orientation observed in shallow crustal rocks in southern Alaska. Geology 18, 737–740.

Brun, J.-P., Sokoutis, G., 2010. 45 M.y of Aegean crust and mantle flow from driven by trench retreat. Geology 38 (9), 815–818.

Brüstle, A., 2012. Seismicity of the Eastern Hellenic Subduction Zone. Ph.D. thesis. Ruhr University, Bochum.

Caputo, R., Pavlides, S., 2013. The Greek Database of Seismogenic Sources (GreDaSS), Version 2.0.0: A Compilation of Potential Seismogenic Sources (Mw & 5.5) in the Aegean Region. http://gredass.unife.it/.

Cochran, E.S., Li, Y., Vidal, J., 2006. Anisotropy in the shallow crust observed around the San Andreas fault before and after the 2004 M6.0 Parkfield earthquake. Bull. Seis. Soc. Am. 96, 364–375. https://doi.org/10.1785/0120050804.

Cossette, E., Audet, P., Schneider, D., Grasemann, B., 2016. Structure and anisotropy of the crust in the Cyclades, Greece, using receiver functions constrained by in situ textural data. J. Geophys. Res. Solid Earth 121, 2661–2678. https://doi.org/10.1002/2015JB012460.

Crampin, S., Chastin, S., 2003. A review of shear wave splitting in the crack-critical crust. Geophys. J. Int. 155, 221–240.

Crampin, S., Peacock, S., 2005. A review of shear-wave splitting in the compliant crack-critical anisotropic. Earth Wave Mot. 41, 59–77.

Crampin, S., Peacock, S., 2008. A review of the current understanding of seismic shear-wave splitting in the Earth's crust and common fallacies in interpretation. Wave Mot. 45, 675–722. https://doi.org/10.1016/j.wavemoti.2008.01.003.

Crampin, S., Peacock, S., Gao, Y., Chastin, S., 2004. The scatter of delay times in shear-wave splitting above small earthquakes. Geophys. J. Int. 156, 39–44. https://doi.org/10.1111/j.1365-246X.2004.02040.x.

Endrun, B., Lebedev, S., Meier, T., Tirel, C., Friederich, W., 2011. Complex layered deformation within the Aegean crust and mantle revealed by seismic anisotropy. Nat. Geosci. 4, 203–207. https://doi.org/10.1038/NGEO1065.

England, P., Houseman, G., Nocquet, J.-M., 2016. Constraints from GPS measurements on the dynamics of deformation in Anatolia and the Aegean. J. Geophys. Res. Solid Earth 121, 8888–8916. https://doi.org/10.1002/2016JB013382.

Evangelidis, C.P., 2017. Seismic anisotropy in the Hellenic subduction zone: effects of slab segmentation and subslab mantle flow. Earth Planet. Sci. Lett. 480, 97–106. https://doi.org/10.1016/j.epsl.2017.10.003.

Evangelidis, C.P., Liang, W.-T., Melis, N.S., Konstantinou, K.I., 2011. Shear wave anisotropy beneath the Aegean inferred from SKS splitting observations. J. Geophys. Res. 116, B04314 https://doi.org/10.1029/2010JB007884.

Floyd, M.A., Billiris, H., Paradisis, D., Veis, G., Avallone, A., Briole, P., McClusky, S., Nocquet, J.-M., Palamartchouk, K., Parsons, B., England, P.C., 2010. A new velocity field for Greece: implications for the kinematics and dynamics of the Aegean. J. Geophys. Res. 115, B10403 https://doi.org/10.1029/2009JB007040.

Friederich, W., Meier, T., 2008. Temporary seismic broadband network acquired data on Hellenic subduction zone. Eos Trans. AGU 89 (40). https://doi.org/10.1029/2008EO400002.

Giannopoulos, D., Sokos, E., Konstantinou, K.I., Tselentis, G.-A., 2015. Shear wave splitting and Vp/Vs variations before and after the Efpalio earthquake sequence, western Gulf of Corinth, Greece. Geophys. J. Int. 200, 1436–1448. https://doi.org/10.1093/gji/ggu467.

Hatzfeld, D., Karagianni, E., Kassaras, I., Kiratzi, A., Louvari, E., Lyon-Caen, H., Makropoulos, K., Papadimitriou, P., Bock, G., Priestley, K., 2001. Shear wave anisotropy in the upper mantle beneath the Aegean related to internal deformation. J. Geophys. Res. 106 (B12), 30737–30753. https://doi.org/10.1029/2001JB000387.

Hu, N., Li, Y., Xu, L., 2020. Crustal seismic anisotropy of the Northeastern Tibetan Plateau and the adjacent areas from shear-wave splitting measurements. Geophys. J. Int. 220, 1491–1503. https://doi.org/10.1093/gji/ggz489.

Huesca-Pérez, E., Valenzuela, R.W., Carciumaru, D., Ortega, R., Gutierrez, E., Cabral-Cano, E., Husker, A., 2019. Margin-wide continental crustal anisotropy in the Mexican subduction zone. Geophys. J. Int. 217, 1854–1869. https://doi.org/10.1093/gji/ggz121.

Johnson, J.H., Savage, M.K., Townend, J., 2011. Distinguishing between stress-induced and structural anisotropy at Mt Ruapehu volcano, New Zealand. J. Geophys. Res. 116, B12303 https://doi.org/10.1029/2011JB008308.

Jolivet, L., Faccenna, C., Piromallo, C., 2009. From mantle to crust: stretching the Mediterranean. Earth Planet. Sci. Lett. 285, 198–209. https://doi.org/10.1016/j.epsl.2009.06.017.

Jolivet, L., et al., 2013. Aegean tectonics: strain localisation, slab tearing and trench retreat. Tectonophysics 587–598, 1–33. https://doi.org/10.1016/j.tecto.2012.06.011.

Kapetanidis, V., Kassaras, I., 2019. Contemporary crustal stress of the Greek region deduced from earthquake focal mechanisms. J. Geodyn. 123, 55–82. https://doi.org/10.1016/j.jog.2018.11.004.

Kaviris, G., Papadimitriou, P., Kravvariti, P., Kapetanidis, V., Karakonstantis, A., Voulgaris, N., Makropoulos, K., 2015. A detailed seismic anisotropy study during the 2011–2012 unrest period in the Santorini Volcanic Complex. Phys. Earth Planet. Interiors 238, 51–88. https://doi.org/10.1016/j.pepi.2014.11.002.

Kaviris, G., Spingos, I., Kapetanidis, V., Papadimitriou, P., Voulgaris, N., Makropoulos, K., 2017. Upper crust seismic anisotropy study and temporal variations of shear-wave splitting parameters in the Western Gulf of Corinth (Greece) during 2013. Phys. Earth Planet. Interiors 269, 148–164. https://doi.org/10.1016/j.pepi.2017.06.006.

Kaviris, G., Spingos, I., Millas, C., Kapetanidis, V., Fountoulakis, I., Papadimitriou, P., Voulgaris, N., Drakatos, G., 2018. Effects of the January 2018 seismic sequence on shear-wave splitting in the upper crust of Marathon (NE Attica, Greece). Phys. Earth Planet. Interiors 285, 45–58. https://doi.org/10.1016/j.pepi.2018.10.007.

Konstantinou, K.I., Evangelidis, C.P., Liang, W.-T., Melis, N.S., Kalogeras, I., 2013. Seismicity, Vp/Vs and shear wave anisotropy variations during the 2011 unrest at Santorini caldera, southern Aegean. J. Volc. Geotherm. Res. 267, 57–67. https://doi.org/10.1016/j.jvolgeores.2013.10.001.

Konstantinou, K.I., Mouslopoulou, V., Liang, W.-T., Heidbach, O., Oncken, O., Suppe, J., 2016. Present-day crustal stress field in Greece inferred from regional-scale damped inversion of earthquake focal mechanisms. J. Geophys. Res. Solid Earth 121. https://doi.org/10.1002/2016JB013272.

Lomax, A., Curtis, A., 2001. Fast, probabilistic earthquake location in 3D models using Oct-Tree importance sampling. Geophys. Res. Abstr. 3.

Lomax, A., Michelini, A., Curtis, A., 2009. Earthquake Location, Direct, Global-Search Methods, in Complexity In Encyclopedia of Complexity and System Science, Part 5. Springer, New York, pp. 2449–2473. https://doi.org/10.1007/978-0-387-30440-3.

Long, M.D., 2013. Constraints on subduction geodynamics from seismic anisotropy. Rev. Geophys. 51, 76–112. https://doi.org/10.1002/rog.20008.

Mardia, K., Jupp, P., 2000. Directional Statistics. John Wiley, Hoboken, New Jersey.

Maupin, V., Park, J., 2007. In: Schubert, G. (Ed.), Theory and Observations: Wave Propagation in Anisotropic media, in Treatise on Geophysics. Elsevier, New York, pp. 289–321. https://doi.org/10.1016/B978-044452748-6.00007-9.

McClusky, et al., 2000. Global positioning system constraints on plate kinematic and dynamics in the Eastern Mediterranean and Caucasus. J. Geophys. Res. 105, 5695–5719.

Mouslopoulou, V., Nicol, A., Begg, J., Oncken, O., Moreno, M., 2015. Clusters of mega earthquakes on upper plate faults control the Eastern Mediterranean hazard. Geophys. Res. Lett. 42, 10282–10289. https://doi.org/10.1002/2015GL066371.

Okaya, D., Vel, S.S., Song, W.J., Johnson, S.E., 2018. Modification of crustal seismic anisotropy by geological structures ("structural geometric anisotropy"). Geosphere 15, 146–170. https://doi.org/10.1130/GES01655.1.

Papazachos, B.C., Karakostas, V.G., Papazachos, C.B., Scordilis, E.M., 2000. The geometry of the Wadati-Benioff zone and lithospheric kinematics in the Hellenic arc. Tectonophysics 319, 275–300.

Paul, A., Karabulut, H., Mutlu, A.K., Saulün, G., 2014. A comprehensive and densely sampled map of shear-wave azimuthal anisotropy in the Aegean-Anatolia region. Earth Planet. Sci. Lett. 389, 14–22.

Peng, Z., Ben-Zion, Y., 2004. Systematic analysis of crustal anisotropy along the Karadere-Düzce branch of the North Anatolian Fault. Geophys. J. Int. 159, 253–274. https://doi.org/10.1111/j.1365-246X.2004.02379.x.

Ranjan, P., Konstantinou, K.I., Andinisari, R., 2019. Spatial distribution of random velocity inhomogeneities in the southern Aegean from inversion of S wave peak delay times. J. Geophys. Res. Solid Earth 124. https://doi.org/10.1029/2018JB017198.

Reilinger, R., McClusky, S., Paradisis, D., Ergintav, S., Vernant, P., 2010. Geodetic constraints on the tectonic evolution of the Aegean region and strain accumulation along the Hellenic subduction zone. Tectonophysics 488, 22–30. https://doi.org/10.1016/j.tecto.2009.05.027.

Saiga, A., Kato, A., Sakai, S., Iwasaki, T., Hirata, N., 2011. Crustal anisotropy structure related to lateral and down-dip variations in interplate coupling beneath the Kii Peninsula, SW Japan. Geophys. Res. Lett. 38, L09307 https://doi.org/10.1029/2011GL047405.

Saltogianni, V., Mouslopoulou, V., Oncken, O., Nicol, A., Gianniou, M., Mertikas, S., 2020. Elastic fault interactions and earthquake rupture along the southern Hellenic subduction plate interface zone of Greece. Geophys. Res. Lett. 47 https://doi.org/10.1029/2019GL086604 e2019GL986604.

Savage, M.K., 1999. Seismic anisotropy and mantle deformation: what have we learned from shear wave splitting? Rev. Geophys. 37 (1), 65–106.

Savage, M.K., Wessel, A., Teanby, N.A., Hurst, A.W., 2010. Automatic measurement of shear wave splitting and applications to time varying anisotropy at Mt Ruapehu volcano, New Zealand. J. Geophys. Res. 115, B12321 https://doi.org/10.1029/2010JB007722.

Schmid, C., Van der Lee, S., Giardini, D., 2004. Delay times and shear wave splitting in the Mediterranean region. Geophys. J. Int. 159, 275–290. https://doi.org/10.1111/j.1365-246X.2004.02381.x.

Shaw, B., Jackson, J., 2010. Earthquake mechanisms and active tectonics of the Hellenic subduction zone. Geophys. J. Int. 181, 966–984. https://doi.org/10.1111/j.1365-246X.2010.04551.x.

Shaw, B., Ambraseys, N.N., England, P.C., Floyd, M.A., Gorman, G.J., Higham, T.F.G., Jackson, J.A., Nocquet, J.-M., Pain, C.C., Piggott, M.D., 2008. Eastern Mediterranean tectonics and tsunami hazard inferred from the AD 365 earthquake. Nat. Geosci. 1, 268–276. https://doi.org/10.0138/ngeo151.

Silver, P., Chan, W., 1991. Shear wave splitting and subcontinental mantle deformation. J. Geophys. Res. 96, 16429–16454.

Sodoudi, F., Kind, R., Hatzfeld, D., Priestley, K., Hanka, W., Wylegalla, K., Stavrakakis, G., Vafidis, A., Harjes, H.-P., Bohnhoff, M., 2006. Lithospheric structure of the Aegean obtained from P and S receiver functions. J. Geophys. Res. 111, B12307 https://doi.org/10.1029/2005JB003932.

Teanby, N., Kendall, J.-M., van der Baan, M., 2004. Automation of shear-wave splitting measurements using cluster analysis. Bull. Seism. Soc. Am. 94, 453–463. https://doi.org/10.1785/0120030123.

Trauth, S.N., 2010. Matlab® Recipes for Earth Sciences, 3rd edition. Springer-Verlag, Berlin/Heidelberg.

Wüstefeld, A., Bokelmann, G., 2007. Null detection in shear wave splitting measurements. Bull. Seism. Soc. Am. 97, 1204–1211. https://doi.org/10.1785/0120060190.

Zoback, M.L., 1992. First- and second-order patterns of stress in the lithosphere: the World Stress Map project. J. Geophys. Res. 97, 11703–11728.